

Approach to canonical pressure profiles in stellarators

Yu.N. Dnestrovskij 1), A.V. Melnikov 1), L.G. Eliseev 1), S.E. Lysenko 1),
K.A. Razumova 1), V.D. Pustovitov 1), A. Fujisawa 2), T. Minami 2), and J.H. Harris 3)

1) Nuclear Fusion Institute, RRC "Kurchatov Institute", Moscow, 123182, Russia,

2) National Institute for Fusion Science, Toki, Japan

3) Fusion Energy Division, Oak Ridge National Laboratory, USA

e-mail contact of main author: dbyn@nfi.kiae.ru

Abstract. Analysis of stellarator database have shown that albeit on many devices the temperature profile consistency is absent, however, on several devices the pressure profiles turn out to be self-consistent. The pressure profile p in the L-mode may be fitted by quasi-linear function: $p_0^{-1} dp/d\rho \sim \text{const} = k = 1.3 \pm 0.1$. To describe the pressure self-consistency we use the variation procedure, previously used for tokamaks. We consider the variation problem to minimize the energy functional W under the constraint that the total plasma current J is a constant. As a result, we obtained the equations for canonical equilibrium and corresponding pressure profiles in L- and H-modes with low, moderate and high magnetic shear. Maximal slopes of these profiles are close to maximal slopes of experimental pressure profiles observed in TJ-II.

1. Introduction

It is well known that the temperature profiles in a tokamak are self-consistent [1-3]. For the stellarators there is no temperature profile consistency [4]. The pressure profile consistency concept works in tokamaks [5]. There was found one example of the pressure profile stiffness in the pellet injection versus gas puff experiment in LHD [6], and also the features of the pressure profile consistency in other LHD experiments [7]. Various examples of pressure profile self-consistency for several stellarators were presented in [8]. In this report we extend experimental database on pressure self-consistency and use the variational procedure developed in [9] for the analysis of the existence of the preferred (canonical) pressure profiles in stellarators.

Plasma temperature and density profile evolution have been considered for the various experiment. NBI heating of on- and off-axis ECRH heated plasma on TJ-II [10], ECRH power scan on W7-AS [11] and CHS [12], high T_i mode on CHS [13], on- and off-axis ECRH on W7-AS [4] and gas puffing on ATF [14] were observed (Table 1). In the TJ-II stellarator, NBI heating ($P_{\text{NBI}} = 300$ kW) of the target ECRH plasma ($P_{\text{ECRH}} = 300$ kW) leads to dramatic changes of the plasma density and temperature. n_e and T_e profile evolution measured by high resolution Thomson Scattering diagnostic is shown in Fig. 1. The values varied up to an order of magnitude, ($0.3 < n_e(0) < 6 \times 10^{19} \text{ m}^{-3}$, $0.2 < T_e(0) < 1 \text{ keV}$), the profiles varied from hollow to peaked (density), and from peaked to flat (electron temperature). In spite of the large difference in n_e and T_e profiles in the analyzed regime, their product, the plasma pressure p_e , presents much stronger profile resilience in the confinement zone of the plasma column. It was found that the normalized pressure profiles $p^{\text{norm}} = p(\rho)/p(0)$ are much less scattered in comparison with plasma n_e and T_e profiles, see Fig. 2.

In the CHS experiments with on-axis $P_{\text{EC}} = 150 \div 215$ kW and density $n_e = 0.47 - 0.95 \times 10^{19} \text{ m}^{-3}$ variation [12], the similar behavior was found: the increase of T_e was accompanied by the decrease of n_e , leaving $p^{\text{norm}}(\rho)$ practically unchanged. In the experiments with the standard major plasma axis ($R_{\text{ax}}=92.1 \text{ cm}$, $n_e(0)=4 \times 10^{19} \text{ m}^{-3}$, $T_e(0) \sim T_i(0)=250 \text{ eV}$), and optimized one

($R_{ax}=87.7\text{cm}$, $n_e(0)=2 \times 10^{19} \text{ m}^{-3}$, $T_e(0)=200 \text{ eV}$, $T_i(0)=130 \text{ eV}$) [13], the same tendency was found, P^{norm} remains almost constant. In high T_i mode ($n_e(0)=1.4 \times 10^{19} \text{ m}^{-3}$, $T_e(0)=700 \text{ eV}$, $T_i(0)=1 \text{ keV}$) [13], p^{norm} almost coincides with the rest of discussed CHS profiles.

In W7-AS experiment with on-axis P_{EC} variation from 0.2 to 0.8 MW at almost the same density $n_e \sim 2 \times 10^{19} \text{ m}^{-3}$ [11], the similar behavior was found: increase of T_e was accompanied by a decrease of n_e , remaining $p^{norm}(\rho)$ practically unchanged. In another experiment, on- and off-axis ECRH alternate with corresponding T_e and n_e variations [4]. It is highlighted in [4] that during off-axis ECRH ($\rho=0.6$) the central density is peaking without an additional particle source, which led to almost unchanged $p^{norm}(\rho)$. At the gas puffing in the ATF [14], the plasma density rise was accompanied by the concordant decay of T_e , again remaining $p^{norm}(\rho)$ practically unchanged.

Despite the difference in the magnetic configurations (heliac TJ-II, torsatrons CHS and ATF, optimized W7-AS), a remarkable similarity is seen in the normalized pressure profiles; in other words, the normalized pressure profile has universal shape for normal confinement (L-mode) in all the observed experiments (Fig. 3). The universal profiles can be fitted by a quasi-linear function in the confinement zone ($0.2 < \rho < 0.8$), $p_0^{-1} dp/d\rho \sim \text{const} = k = p_0^{-1} \Delta p_{linear} / \Delta \rho_{linear}$, where $\Delta \rho_{linear}$ is the radial extension, where profile has almost linear shape. In the observed cases $\Delta \rho_{linear} \sim 0.6$, $k \approx 1.3 \pm 0.1$ (see TABLE 1).

Contrary to the L-mode, pressure profiles show different shapes during improved confinement modes. An example of the edge transport barrier is shown in Fig 2(b); $p^{norm}(\rho)$ in HDH confinement mode in W7-AS strongly differs from the universal profile, while the reference Normal Confinement profile belongs to the universal one [15]. In case of the ITB formation the pressure profiles have clearly two components. Outside the ITB, the pressure profiles show strong similarity (the universal profile takes place), while in the ITB area $p_0^{-1} dp/d\rho$ is significantly higher. Figure 3 shows W7-AS data with on-axis $P_{EC} = 1.2 \text{ MW}$, where the temperature and pressure profiles show the ITB formation at $\rho \sim 0.25$ [11]. In the CHS the more pronounced ITB was obtained for the high power on-axis ECRH at $\rho \sim 0.4$ [13]. Again, outside the ITB area the profiles coincide with the universal one.

TABLE 1. FITTING RESULTS OBTAINED FROM DIFFERENT STELLARATORS.
 Δk is linear regression error for k .

Device	Type	R , m	a , m	B , T	$\nu/2\pi(a)$	$-k$	Δk	Regime, [Ref.]
TJ-II	heliac	1.5	0.22	1.0	1.6, low shear	1.34	0.04	EC on axis+NBI [10]
						1.39	0.04	EC off- +NBI [10]
W7-AS	modular coils	2.0	0.2	2.5	low shear, 0.56	1.19	0.02	P_{EC} scan, n_e const [11]
			0.16			1.28	0.02	EC on- off-axis [4]
			0.13			1.38	0.02	HDH [15]
CHS	torsatron	0.92	0.19	0.9	high shear	1.32	0.02	EC on- +NBI [12]
				1.9		1.39	0.02	EC on-, ITB [13]
				1.9		1.36	0.02	High T_i [13]
ATF	torsatron	2.1	0.27	1.9	shear	1.11	0.02	gas puff [14]

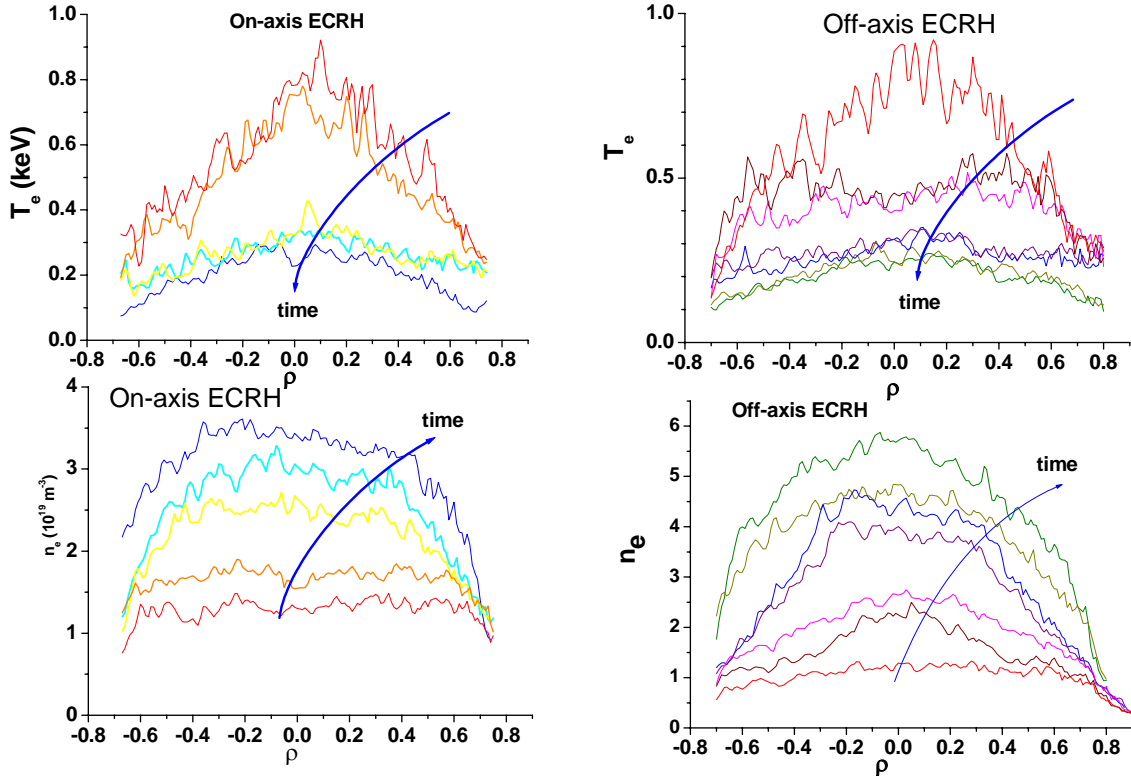


FIG. 1. T_e (upper) and n_e (lower) profile evolution in the NBI experiments for on-axis (left) and off-axis (right) ECRH in TJ-II.

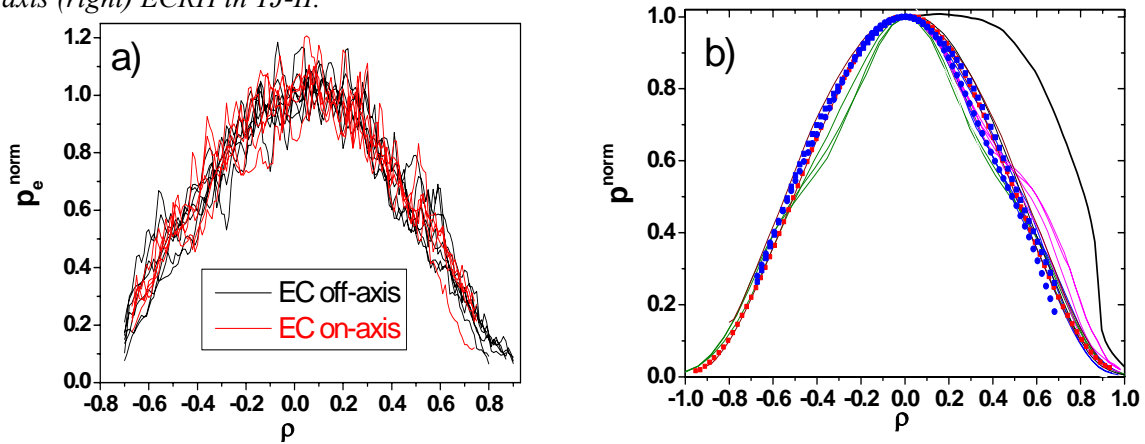


FIG 2. a) TJ-II normalized pressure profiles for data from FIG.1, b) $p^{norm}(\rho)$ for the data presented in TABLE forms the universal profile; **CHS**: red dots – high Ti mode, brown – R_{ax} variation, red – P_{EC} variation, **ATF**: purple - gas puff, **W7-AS**: green - P_{EC} -on scan, blue – EC on- and off-axis, black – HDH-mode, dark blue – reference Normal Confinement mode, **TJ-II**: blue dots – EC on, off. Profiles from all machines and experiments were radially normalized to the actual plasma size, $p^{norm}(1)=0$.

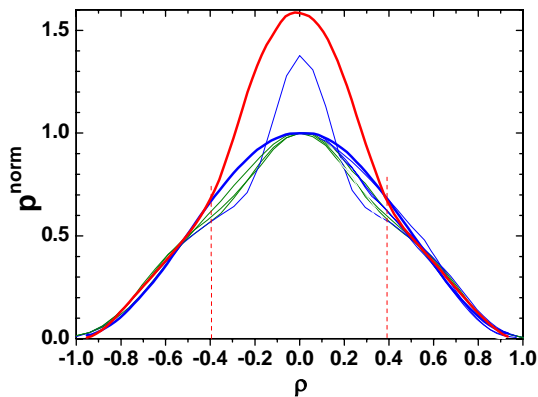


FIG. 3. The universal profile exists outside the ITB area. **CHS**: fat blue – high Ti mode, fat red – ITB, **W7-AS**: green – $P_{EC}=0.2-0.8$ MW, thin blue – ITB ($P_{EC}=1.2$ MW). Dashed lines designate internal transport barrier.

To summarize the empirical observation, we may conclude: (I) In spite of large variety in the profiles of plasma electron temperature and density, their product, the electron pressure presents the feature of profile constancy in stellarator devices in observed experiments with wide range of the plasma and heating parameters.

(II) In the L-mode plasmas of the medium size stellarators the pressure profiles show remarkable similarities between each other in low (TJ-II, W7-AS) and high (CHS, ATF) magnetic shear configurations. So, the universal profile, characterized by $p_0^{-1} dp/d\rho \sim \text{const} = k$, was found for L-mode plasmas and out of the ITB area. The other types of profile like LHD case [6] may take place for specific plasma conditions.

(III) The observation of the universal constant k in the L-mode (e.g. in the absence of strong $\mathbf{E} \times \mathbf{B}$ effects) may suggest that the turbulence and the associated transport reach some kind of saturation level, which does not depend on the absolute values of T_e and n_e , but alternative explanations (e.g. based on the role of atomic physics and links between magnetic configuration and gradient) cannot be excluded. The validation of the transport-based hypothesis would require to characterize the link between local gradients and turbulent transport.

2. Canonical pressure profiles

We start from the energy integral

$$W = \int_V \left(\frac{\mathbf{B}^2}{2} + \frac{p}{\gamma-1} \right) dV, \quad (1)$$

where \mathbf{B} is the magnetic field, p is the plasma pressure, γ is the ratio of specific heats, and the integration is performed over the plasma volume. First, we integrate here over the toroidal angle ζ , so that W will be transformed into the integral over the axially symmetric toroid \bar{V} inside the toroidally averaged plasma boundary. In conventional stellarators with planar circular axis, all physical quantities can be represented as

$$f = \bar{f} + \tilde{f} \quad (2)$$

where $\bar{f}(r, z)$ is the axially symmetric (or toroidally averaged) part of f , and $\tilde{f}(r, z, \zeta)$ is its oscillating part, (r, z, ζ) are the usual cylindrical coordinates with z -axis directed along the main axis of the system. Accordingly,

$$\mathbf{B} = \bar{\mathbf{B}} + \tilde{\mathbf{B}}, \quad \bar{\mathbf{B}} = B_t \mathbf{e}_\zeta + \mathbf{B}_p, \quad (3)$$

where $\bar{\mathbf{B}}$ is the axially symmetric and $\tilde{\mathbf{B}}$ is the helical magnetic field, \mathbf{e}_ζ is the unit vector in the toroidal direction, B_t is the toroidal component of $\bar{\mathbf{B}}$ and \mathbf{B}_p is the poloidal magnetic field. It is shown in [17] that

$$\int_V \mathbf{B}^2 dV = \int_{\bar{V}} (\bar{\mathbf{B}}^2 - \tilde{\mathbf{B}}^2) d\bar{V}. \quad (4)$$

With this relation we obtain

$$W = \int_{\bar{V}} \left(\frac{\bar{\mathbf{B}}^2 - \tilde{\mathbf{B}}^2}{2} + \frac{\bar{p}}{\gamma-1} \right) d\bar{V}, \quad (5)$$

where \bar{p} is the axially symmetric part of p , or averaged plasma pressure. To simplify the notations we further use p instead of \bar{p} . In (5) the integration is performed over the 2D ‘‘quasi-tokamak’’ region \bar{V} .

To calculate the variation of the energy, δW , we need $\delta \bar{\mathbf{B}}^2$. The axially symmetric poloidal field can be described as $\mathbf{B}_p = \text{rot} A_t \mathbf{e}_\zeta$. Therefore

$$\delta \frac{\mathbf{B}_p^2}{2} = \text{div} \delta A_t (\mathbf{e}_\zeta \times \mathbf{B}_p) + j_\zeta \delta A_t, \quad (6)$$

where j_ζ is the ζ -averaged toroidal component of the current density: $j_\zeta = \mathbf{e}_\zeta \cdot \text{rot} \mathbf{B}_p$.

With (6) we obtain from (5)

$$\delta W = \int_{\bar{V}} \left(B_t \delta B_t + j_\zeta \delta A_t + \frac{\delta p}{\gamma - 1} \right) d\bar{V}. \quad (7)$$

We assumed here that the helical field is fixed (is not varied). In stellarators we have [17]

$$\mathbf{B}_p = \frac{1}{2\pi} [\nabla(\psi - \psi_v) \times \nabla \zeta], \quad r A_t = \frac{\psi - \psi_v}{2\pi}. \quad (8)$$

Here ψ_v is the poloidal flux of the helical field $\tilde{\mathbf{B}}$.

In [16] the energy was minimized under the constraint that the total plasma current is a constant of motion, $\delta J = 0$. Following this approach we consider the variation problem for the functional

$$\Phi = W - \lambda J, \quad (9)$$

where λ is the Lagrange multiplier. The net toroidal current is

$$J = \int_{S_\perp} \mathbf{j} d\mathbf{S}_\perp = \int_{\bar{S}_\perp} j_\zeta d\bar{S}_\perp = \int_{\bar{V}} \frac{j_\zeta}{2\pi r} d\bar{V}, \quad (10)$$

where S_\perp is the toroidal cross-section of the plasma and \bar{S}_\perp is its ζ -averaged image, with $d\bar{V} = 2\pi r d\bar{S}_\perp$. Then

$$\delta W - \lambda \delta J = \int_{\bar{V}} \left(B_t \delta B_t + \frac{j_\zeta}{r} \delta(r A_t) - \lambda \frac{\delta j_\zeta}{2\pi r} + \frac{\delta p}{\gamma - 1} \right) d\bar{V}, \quad (11)$$

and the variation principle with (9) gives the following Euler equation:

$$B_t \frac{\partial B_t}{\partial \psi} + \frac{j_\zeta}{2\pi r} - \frac{\lambda}{2\pi r} \frac{\partial j_\zeta}{\partial \psi} + \frac{p'(\psi)}{\gamma - 1} = 0. \quad (12)$$

where prime means the derivative with respect to ψ .

In stellarators with $|\tilde{\mathbf{B}}/B_t| \ll 1$ we have [17]

$$B_t = \frac{F(\psi)}{2\pi r} \quad \text{and} \quad j_\zeta = \frac{FF'(\psi)}{2\pi r} + 2\pi r \frac{dp}{d\psi} (1 + \Omega^0), \quad (13)$$

Here $\Omega^0 = \langle \tilde{\mathbf{B}}^2 \rangle_\zeta / B_0^2$ with $\langle \dots \rangle_\zeta$ staying for the toroidal averaging, and B_0 is the toroidal magnetic field at the axis. The quantity Ω^0 can play an important role in some special cases when it can be as large as the inverse aspect ratio with strong in-out asymmetry on the magnetic surfaces. But usually $\Omega^0 \ll 1$ so it can be disregarded in (13). With (13) equation (12) turns into

$$\frac{2FF' - \lambda(FF')'}{4\pi^2 r^2} + (p' - \lambda p'')(1 + \Omega^0) + \frac{p'}{\gamma - 1} = 0, \quad (14)$$

The second and the third terms in (14) are constant at the magnetic surfaces while the first term is not constant if nominator is not equal to zero. So disregarding Ω^0 we obtain finally

$$2FF' - \lambda(FF')' = 0, \quad \gamma p' - \lambda(\gamma - 1)p'' = 0, \quad (15)$$

We put further that $\gamma = 5/3$, $\gamma/(\gamma - 1) = 5/2$. The equations (15,21)-(16,22) imply that

$$FF' = C_F \exp(2\psi/\lambda), \quad p' = C_p \exp(2.5\psi/\lambda). \quad (16)$$

With these functions the two-dimensional equilibrium equation for stellarators [17] becomes

$$\operatorname{div} \frac{\nabla(\psi - \psi_v)}{r^2} = -2\pi j / r = -4\pi^2 C_p \exp(2.5\psi/\lambda) - C_F \frac{\exp(2\psi/\lambda)}{r^2}. \quad (17)$$

The latter equation can be naturally called *Canonical equilibrium equation* for conventional stellarators. The equation (17) is of Poisson type equation, which requires the boundary condition at the plasma boundary S , which is a magnetic surface,

$$\psi(S) = \text{const} = \psi_b. \quad (18)$$

Equation (17) includes three parameters, C_F , C_p and λ , so we have to add three additional conditions to find them. One can be the prescription of ψ at the magnetic axis,

$$\psi(M_0) = \psi_0, \quad (19)$$

or this can be replaced by the given value of the rotational transform $\mu = d\psi/d\Phi$ at the magnetic axis. Here $\Phi = \int_{S_\psi} B_t dS$ is the toroidal flux inside the magnetic surface ψ .

The second constraint is the given total plasma current:

$$J = \int_{S_\perp} \mathbf{j} b d\mathbf{S}_\perp. \quad (20)$$

In stellarators this is usually small, and often $J = 0$ is assumed. In experiments we usually know the averaged β (the ratio of plasma pressure to magnetic pressure). It can also be represented in the model by

$$\beta_0 = 2p_0 / B_0^2, \quad (21)$$

where p_0 is the plasma pressure at the magnetic axis and B_0 is the toroidal field at the axis. Prescription of β_0 can be the third required condition.

Complete solution of the canonical equation (17) would give us the parameter λ , which was introduced as the Lagrange multiplier in (9). With known λ we could find the profiles of F and p , which for the canonical equilibrium are determined by the one-dimensional equations (16). The solution for pressure p can be written as

$$p = (p_0 - p_b) \frac{e^{1.25ku} - e^{1.25k}}{1 - e^{1.25k}} + p_b, \quad (22)$$

where p_0 and p_b are the plasma pressures at the magnetic axis and at the edge, respectively,

$$u = \frac{\psi - \psi_0}{\psi_b - \psi_0} \quad (0 < u < 1) \quad k = \frac{2}{\lambda} (\psi_b - \psi_0). \quad (23)$$

A general solution to Eq. (17) is

$$\psi = \psi_v + \psi_{ext} + \psi_{pl}, \quad (24)$$

where ψ_{ext} describes the contribution due to the external poloidal field and ψ_{pl} due to the equilibrium currents in the plasma. We assume here $\psi_{ext} = 0$ and consider the case

$|\psi_{pl}| \ll |\psi_v|$, which corresponds to low- β plasma. Then

$$\psi \approx \psi_v. \quad (25)$$

Let us consider the simplest case of the cylindrical plasma with circular cross-section. In this case $\psi_v = \psi_v(\rho)$, where ρ is the radial coordinate of the plasma cross-section. Then

$$\partial\psi_v / \partial\rho = -2\pi\rho B_0 \mu, \quad (26)$$

where μ is the rotational transform which, in a general case, can be approximated by

$$\mu = \mu_0 + (\mu_b - \mu_0)\xi^2 \quad (27)$$

with $\mu_0 = \mu(0)$, $\mu_b = \mu(1)$, $\xi = \rho/b$ and b is the minor radius, so that $0 \leq \xi \leq 1$. This yields

$$\psi_v = -\pi B_0 b^2 \xi^2 \left[\mu_0 + (\mu_b - \mu_0)\xi^2 / 2 \right] \quad u = \xi^2 \frac{2\mu_0 + (\mu_b - \mu_0)\xi^2}{\mu_0 + \mu_b}. \quad (28)$$

This can be called the low- β approximation of u .

With given p_b/p_0 and u we have the last unknown k . As a particular example let us consider the case with the prescribed ratio $p_b/p_0 = e^{1.25k}$ i.e $k = -4/5 \ln(p_0/p_b)$. This choice corresponds to the following boundary condition

$$\frac{1}{p} \frac{dp}{du}(u=1) = 1.25k, \quad (29)$$

Such a type of boundary condition was proposed for tokamaks by Kadomtsev in his interpretation of the variation procedure [18]. The condition (29) gives

$$p = p_0 \exp(1.25ku). \quad (30)$$

Expression (30) with u given by (28) reduces to

$$p_c(\xi) = p_0 \exp \left\{ -2 \left[\ln \left(\frac{p_0}{p_b} \right) / \left(1 + \frac{\mu_b}{\mu_0} \right) \right] \xi^2 \left[1 + \left(\frac{\mu_b}{\mu_0} - 1 \right) \xi^2 / 2 \right] \right\} \quad (31)$$

which can be called as a Kadomtsev-type profile for stellarators.

We consider the models of H- and L-modes, using the freedom in selecting the parameter p_0/p_b describing the plasma,

$$p_0/p_b = 10 \quad (\text{for the H-mode}), \quad p_0/p_b = 100 \quad (\text{for the L-mode}), \quad (32)$$

and 3 cases with different shear, which is a characteristic of a stellarator configuration

$$\mu_b/\mu_0 = 1 \text{ (zero shear)}, \quad \mu_b/\mu_0 = 2 \text{ (moderate shear)}, \quad \mu_b/\mu_0 = 4 \text{ (large shear)} \quad (33)$$

Substituting (32)-(33) into (31) we can find the largest slope coefficients $k =$

$\max [-(1/p_0) dp_c/d\xi]$ of the profiles of $p(\xi)/p_0$. The results are shown in figure 3. This shows $1.45 < k < 1.55$ for the L-mode and $k = 1.3$ for the H-mode. It was shown earlier in Table 1 that $k = 1.3 \pm 0.1$ for the experimentally measured L-mode pressure profiles in several devices. The proximity of these experimental results and the above theoretical estimations lead to the conclusion that the observable experimental self-consistency of pressure profiles in stellarators might be based on the minimum energy variation principle. Note that the representation of pressure profiles in the exponential form similar to (31) was used recently during the analysis of the LHD experimental profiles [12].

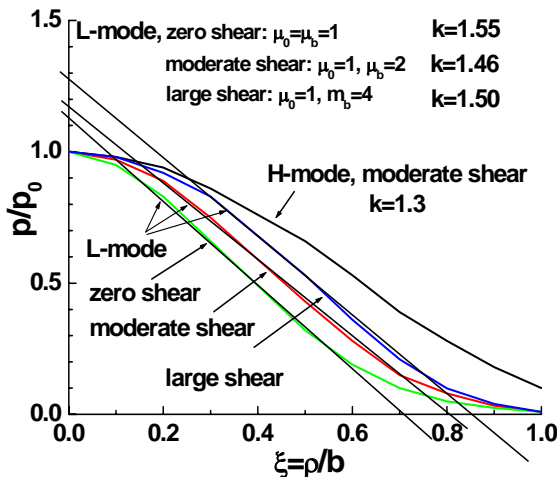


FIG. 4. The canonical pressure profiles for stellarators with different magnetic configuration. Here $k = \max [-(1/p_0) dp_c/d\xi]$.

3. Conclusion

It was assumed for a long time that the energy and particle transport in a stellarator is defined in main by neoclassical transport coefficients and in this sense the stellarator differs radically from a tokamak, where the transport is anomalous and defined by the plasma turbulence. Nevertheless, gradually, the experimental facts originated the doubt in such a paradigm. The observation of the H-mode and internal transport barriers and the proximity of the stellarator energy confinement time scaling to the tokamak scaling led to the opinion that the turbulent transport plays the important role in stellarators. It was reported recently [7] that the pressure profile self-consistency is observed in stellarators, as well.

In this Report the variation procedure (proposed 20 years ago for tokamaks) is used to construct the pressure canonical profiles for stellarators. As a result we come to the two-dimensional equilibrium equation for so called “canonical equilibrium”. The corresponding pressure profiles are estimated in low- β plasma approximation. The profiles thus obtained are close to the experimental normalized pressure profiles, although slightly differ from them as in tokamak case. However, in tokamaks the temperature profiles of electrons and ions are self-consistent also, which does not seen so far in stellarators. Apparently, this difference is explained by the absence of the total current in stellarator and, as a consequence, by a smaller influence of Ohm’s law. As a result in a stellarator the temperature profile easily changes its form but this feature is quite limited in a tokamak. The existing of two self-consistent profiles in a tokamak (temperature and pressure) allows one to construct the transport model concerning the temperatures and plasma density based on this property [5,19]. Unfortunately the second self-consistent profile for the stellarator is not seen so far, so the problem of full canonical profiles transport model for stellarator remains open.

Acknowledgments

Kurchatov team was supported by Grants RFBR 08-02-01326 and 07-02-01001, INTAS 100008-8046. Authors thank C. Hidalgo and F. Wagner for useful discussions.

References

- [1] COPPI, B., Comments Plasma Phys. Control. Fusion **5** (1980) 261.
- [2] ESIPTCHUK, Yu.V., RAZUMOVA, K.A., Plasma Phys. Control. Fusion **28** (1986) 1253.
- [3] RYTER, F., et al., Plasma Phys. Control. Fusion **43** (2001) A323.
- [4] WAGNER, F., et al., Phys. Plasmas **12** (2005) 072509.
- [5] DNESTROVSKIJ, Yu.N. et al., Nucl. Fusion **46** (2006)953
- [6] YAMADA, H. et al., Nucl. Fusion **41** (2001) 901.
- [7] MIYAZAWA, J. J. Plasma Fusion Res. **81** (2005) 302.
- [8] MELNIKOV, A V et al., 2007 34-th EPS Plasma Physics Conf. Rep. P2.060.
- [9] DNESTROVSKIJ, Yu.N. et al., submitted to Plasma Phys. Control. Fusion.
- [10] LINIERS, M. et al., 15 ISW, Madrid, 2005, P3-14.
- [11] ERCKMANN, V. et al., In: “Radio Frequency Power in Plasmas”, AIP (1999)
- [12] NAKANO, H. Private communication.
- [13] OKAMURA, S. et al., Nucl. Fusion **39** (1999) 1337
- [14] SHATS, M. et al., Phys. Plasmas **2** (1995) 398.
- [15] MCCORMICK, K., Phys. Rev. Lett. 89 (2002) 015001
- [16] HSU, J.Y., CHU, M.S., Phys. Fluids **30** (1987) 1221.
- [17] PUSTOVITOV, V.D., in Reviews of Plasma Physics (KADOMTSEV, B.B. and SHAFRANOV, V.D. Ed.), Consultants Bureau, New York) **21** 2000 1.
- [18] KADOMTSEV, B.B., Sov. J. Plasma Phys. **13** (1987) 443.
- [19] DNESTROVSKIJ, Yu. N. et al., Plasma Phys. Control. Fusion **49** (2007) 1477.